Journal of Molecular Graphics and Modelling 28 (2009) 62–69

Contents lists available at ScienceDirect

Journal of Molecular Graphics and Modelling

journal homepage: www.elsevier.com/locate/JMGM

Gas sensing properties of platinum derivatives of single-walled carbon nanotubes: A DFT analysis

P. Pannopard [a,b], P. Khongpracha [a,b], M. Probst [c], J. Limtrakul [a,b,*]

[a] Laboratory for Computational & Applied Chemistry, Chemistry Department, Faculty of Science, Kasetsart University, Bangkok 10900, Thailand
[b] Center of Nanotechnology, Kasetsart University Research and Development Institute, Kasetsart University, Bangkok 10900, Thailand
[c] Institute of Ion Physics and Applied Physics, Innsbruck University, Technikerstraße 25, 6020 Innsbruck, Austria

ARTICLE INFO

Article history:
Received 31 October 2008
Received in revised form 23 March 2009
Accepted 11 April 2009
Available online 20 April 2009

Keywords:
Sensor
NO_2
NH_3
Pt–CNT assemblies
Defected CNTs
DFT

ABSTRACT

The limitations of intrinsic carbon nanotube (CNT) based devices to examine toxic gases motivate us to investigate novel sensors which can possibly overcome sensitivity problems. Pt–CNT assemblies (with Pt deposited externally as well as internally Pt-doped ones) interacting with NO_2 and NH_3 are studied and compared with unmodified CNTs. DFT calculations show that Pt can enhance adsorption and charge transfer processes to a very large degree. Incoming gas molecules cause changes in the electronic structure and charge distribution of the Pt-substituted CNTs that are both larger and more far-reaching than in their unmodified counterparts. Their relatively high stability is unaffected by the complexation with NO_2 and NH_3. CNTs with defective surface were also investigated. The sensing performance of Pt-doped CNT is found to be superior to defected CNTs.

1. Introduction

Chemical sensors based on nanowires of semiconducting single-walled carbon nanotubes (SWCNTs) that perform well have been utilized for detecting pollutant and toxic gases like NO_2 and NH_3. Such nano-scale assemblies can achieve high sensitivity and fast response times, even at ambient temperature [1]. The fundamental sensing mechanism for these devices is the modulation of the conductivity of the SWCNT as a result of the charge transfer between it and analyzed gas. Former computational studies indicate that both NO_2 and NH_3 are physisorbed on unmodified-CNT surfaces, causing only a small charge transfer and mildly triggered conductance responses [2–5].

Therefore, there were many attempts to elucidate why experimentally strong signals are observed. Eventually, there are still several assumptions involved. Concerning NO_2 and NH_3, an indirect mechanism is regularly proposed. For instance, in the case of NO_2, NO_3 formation by the reaction of NO_2 with pre-adsorbed oxygen species or, for NH_3, activation by water vapor [1,3], is assumed to be the first step. Such complicated phenomena generally exclude the rational design of improved sensors. We did not consider them when we investigated modified CNTs with respect to their NO_2 and NH_3 sensing capabilities as discussed below.

Amongst the many possible strategies to tailor the selectivity and sensitivity of CNTs, the generation of new active sites on their surface is classically the premier strategy to overcome the drawback of the intrinsically inert CNT structure. The introduction of structural defects on the walls of CNTs, especially ones associated with vacancies, can be expected to enhance the sensitivity for small molecules like NO_2 and NH_3 [6–8]. Furthermore, embedding of foreign atoms or doping makes it possible to detect a wide range of gases by altering the dopants. B-, N- and Al-doped SWCNTs have proven to be highly sensitive to NH_3, NO_2, CO, H_2O and HCOH [9–12]. Interestingly, the so-called decoration of a SWCNTs network with various transition metals allows the fabrication of single-chip devices [13]. This can enlarge the diversity of identified molecular species by combining CNTs decorated with different metals, each for one particular gas. Recent reports impart that the deposited metal–CNTs exhibit enhanced sensitivity, compared to bare CNTs [14]. For example, Pt- and Au-functionalized MWCNTs are more sensitive by an order of magnitude for NH_3 and NO_2 detection. Not only the catalytic role but also the engineering of transducer platforms are vital for sensor development. Typically, the efficiency of sensory support strongly depends on the amount of active locus on the surface which can boost the reactivity and sensitivity. In particular, for the metal–CNTs hybrid scaffold, the generation of small size metal clusters

* Corresponding author at: Laboratory for Computational & Applied Chemistry, Chemistry Department, Faculty of Science and Center of Nanotechnology, Kasetsart University Research and Development Institute, Kasetsart University, Bangkok 10900, Thailand. Tel.: +66 256 25555x2169; fax: +66 256 25555x2176.
E-mail address: jumras.l@ku.ac.th (J. Limtrakul).

1093-3263/$ – see front matter © 2009 Elsevier Inc. All rights reserved.
doi:10.1016/j.jmgm.2009.04.005

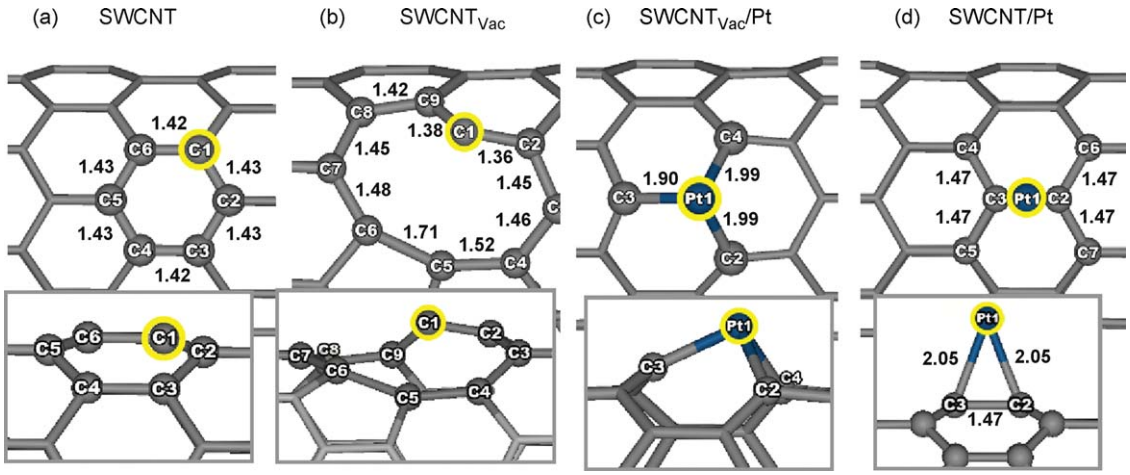

Fig. 1. (a) pristine SWCNT, (b) vacancy SWCNT, (c) Pt-doped SWCNT and (d) Pt-deposited SWCNT. Side views are shown under corresponding pictures. The yellow marks indicate the active site studied for the SWCNTs (a–d). Atom–atom distances (Å) around the active centers are also depicted.

with high content and uniform distribution is indeed realized. The surface adsorption of metal clusters on CNT-sidewalls is a well-known technique in sensing technology [13–16], nevertheless the large size of the metal clusters on the CNT produced by this technique often leads to an unfavorably small specific surface. Recent experiments and calculations indicate that defective CNTs are also capable of improving the Pt loading content and size distribution [17], and also that Pt atoms prefer to adsorb on a vacancy site, resembling conventional doping. Impurity doping works by changing the local chemical reactivity. Pt itself is well-known for its adsorption capabilities of small molecules [18–21]. We compare corresponding properties of pristine SWCNTs, of SWCNT with vacancies ($SWCNT_{Vac}$) and with Pt-deposited on perfect SWCNT (SWCNT/Pt). Ammonia (NH_3) and nitrogen dioxide (NO_2) have been chosen because of their importance as pollutants and industrial toxicants and also because they are good models for electron donors and electron acceptors, respectively.

2. Methodology

Fully optimized geometries and the properties of the systems were derived by means of density functional calculations in the spin-unrestricted generalized gradient approximation by using the DMol^3 code [22,23] with double-numerical polarized (DNP) basis sets. Concerning the density functional we faced certain restrictions with respect to CPU time and the implementation of periodic boundary conditions. This prohibits, for example, using new density functionals like MPWB1K [24–26]. Our calculations were performed with the PW91 [27] density functional which, while not including dispersion energy contributions, can efficiently be applied to large periodic systems. It has been used on a large number of comparable systems in good agreement with experimental information. The interactions between core and valence electrons are represented by DFT semicore pseudopotentials [28]. The real-space orbital cutoff was set to 4.0 Å, the force threshold for optimizations was 0.01 eV and the Brilloiouin zone *k*-point sampling was performed in a $1 \times 1 \times 2$ Monkhorst–Pack mesh [29]. These values of the parameters correspond to a medium-quality calculation which delivers the highest accuracy still computationally feasible for such large systems. Periodic-boundary conditions were applied with a tetragonal unit cell of $20 \times 20 \times 12.78$ Å^3. This is large enough to virtually avoid interactions with images in neighboring cells. An (8,0)SWCNT with 96 carbon atoms was chosen as a model of an unmodified SWCNT. This is a semiconducting SWCNT, a feature that is necessary for the sensor circuit. For this model, we calculated a HOMO–LUMO energy gap of 0.63 eV which agrees well with previous DFT studies [30,31]. From this SWCNT, the models for the Pt-deposited, and Pt-doped, and SWCNTs with vacancy defects were derived. They are shown and explained in Fig. 1.

We investigated different sites of the gas molecules above the hexagonal carbon ring structure of the CNT. NO_2 was oriented parallel or perpendicular to the SWCNT surface. For the latter one, we considered three orientations with N pointing to the SWCNT, with a single O atom or both O atoms pointing to the SWCNT. Likewise, NH_3 was placed above a carbon atom, between two carbons and above the center of a hexagonal ring. For each case, N, one H atom or all three H atoms were oriented towards the CNT surface. The N–H bonds were parallel to the hexagonal carbon framework or rotated away by 60°. Detailed graphs of the initial and optimized structures are available as supplementary information (S1 and S2, respectively).

The binding energies between the gas molecules and the SWCNT were calculated according to:

$$E_b = E_T(\text{support} : \text{gas}) - E_T(\text{support}) - E_T(\text{gas})$$

where E_T (support:gas) is the total energy of a gas molecule adsorbed on the active site of support and E_T (support) and E_T (gas) are the total energies of the support and the gas molecule, respectively. All E_T values refer to quantum chemical energies at optimized geometries. The electronic structure of the energetically most favorable complexes was analyzed in order to estimate the sensing susceptibility with respect to the following properties: partial and net charge transfers were obtained from a Mulliken population analysis. The partial and total density of states (PDOSs and DOSs) were calculated and the frontier molecular orbitals were analyzed. Electron density difference maps of optimized structures were calculated with a plane-wave basis set and ultrasoft pseudopotentials [32] as implemented in the CASTEP program [33].

3. Results and discussion

3.1. Energetics and optimized geometries

We start by considering the optimized geometries of pristine, defective, Pt-doped and Pt-deposited SWCNTs (Fig. 1) which serve as the sensing platforms. Fig. 1a shows the common SWCNT with a typical C–C bond length of about 1.42 Å and a nanotube diameter of 6.38 Å closely matching that of previous studies [30]. In Fig. 1b,

Table 1
Binding energies E_b between Pt and SWCNT and $SWCNT_{Vac}$ and binding energies of NO_2 and NH_3 to the four types of SWCNTs. The structures are shown in Figs. 2 and 3, respectively. The energies are given in kcal/mol.

Sensing support		E_b (SWCNT/Pt)
$SWCNT_{Vac}$/Pt		163.62
SWCNT/Pt		53.39
Sensing support	**E_b (support:NO_2)**	**E_b (support:NH_3)**
SWCNT	1.96	1.33
$SWCNT_{Vac}$	55.90	2.76
$SWCNT_{Vac}$/Pt	50.91	30.52
SWCNT/Pt	34.92	40.96

the single vacancy defected SWCNT is shown. It results from the 12-membered ring created by removing one carbon atom from the graphene sheet and the subsequent reconstruction to a 5-membered ring and a 9-membered ring. It holds one unsaturated carbon (C1), slightly sticking out from the tube surface. The rearrangement deforms the structure to obtain an elliptical cross section with major and minor diameters of 6.56 Å and 6.17 Å, respectively. Doping of the large Pt atom to the vacancy (Fig. 1c) causes a deformation of the nearby hexagonal rings in the doping region. The Pt–C distance is 1.9 Å and Pt protrudes outside of the SWCNT surface. Even though in this structure the SWCNT is apparently distorted (elliptic diameters: 6.49 Å and 6.28 Å), the Pt atom is bound with 163.62 kcal/mol (Table 1). This value is similar to the one reported in [17]. This stabilization can be ascribed to the saturation of the dangling C bonds and the formation of stable hexagonal rings. Consequently, the binding energy in Pt-deposited SWCNT is smaller (53.39 kcal/mol). Fig. 1d shows the energetically most favorable conformation with Pt residing above the C2–C3 bond [34–35] with a Pt–C distance of 2.05 Å. The geometry of the tube is changed due to strong Pt–CNT interaction causing nonidentical diameters with 6.48 Å and 6.29 Å of the longest and the shortest ones, respectively. In a long-lived sensor, the attachment of Pt to the SWCNT must be stable enough to withstand temperature and environmental effects. Although this is difficult to quantify, also the Pt-deposited SWCNT should still be a stable enough device.

3.1.1. NO_2

The most stable optimized geometries, their geometrical parameters and the binding energies of NO_2 adsorption on each support are given in Fig. 2 and Table 1. Nevertheless, there are some experimental and computational studies revealing that the nitro derivative on fullerenes can be found [36,37]. Though, due to the chemically inert CNT system, the functionalization of NO_2 on the CNT sidewall should be more difficult than that of a fullerene surface. One can see that the NO_2 molecule is merely physisorbed on the pristine SWCNT with the lowest absorption energy (1.96 kcal/mol) and a distance of 3.11 Å between N and C. The monomer geometries of the SWCNT and the NO_2 molecules are undisturbed.

In $SWCNT_{Vac}$, the unsaturated carbon atom (C1) binds to the nitrogen atom of NO_2 (r_{C-N} = 1.46 Å) with an interaction energy of 55.90 kcal/mol. The binding can be attributed to the under-coordinated carbon atoms near the vacancy. C1 is the most negatively charged carbon and attracts the partially positively charged N atom of NO_2. Excess electrons are located in the antibonding orbitals of the NO_2 molecule causing a change of the N–O distance from 1.21 Å to 1.24 Å, The stability of the $SWCNT_{Vac}$/Pt:NO_2 complex (50.91 kcal/mol) is similar to that of $SWCNT_{Vac}$. Pt bonds to both oxygens of NO_2 causing an elongation of the N–O bond to 1.28 Å. The interaction between NO_2 and the Pt atom in SWCNT/Pt:NO_2 is similar to the one described above. In our SWCNT/Pt:NO_2 model, the SWCNT–Pt distances increased from 2.05 Å to 2.11 Å after NO_2 binding, indicating that the strong binding of NO_2 (34.92 kcal/mol) comes at the expense of a destabilization of the Pt–SWCNT stability.

3.1.2. NH_3

The most stable optimized geometries of NH_3 adsorbed on each support are shown in Fig. 3, together with the relevant distances. Their binding energies are tabulated in Table 1. In agreement with previous studies [5,9] in the preferred orientation, the hydrogen atoms of NH_3 point towards the SWCNT (Fig. 3a). NH_3 is noncovalently bound with only 1.33 kcal/mol and a C–H distance of about 3.3 Å. In contrast to NO_2, the interaction in $SWCNT_{Vac}$:NH_3 is only slightly stronger (2.76 kcal/mol) because in both cases a hydrogen bonded interaction is the only possibility. Here, the more negatively charged C1 acts as the electron donor and a C···H–N hydrogen bond can be formed (Fig. 3b). These weak interactions mean that materials consisting of both SWCNT and $SWCNT_{Vac}$ are inappropriate sensing platforms for NH_3 detection. In $SWCNT_{Vac}$/Pt:NH_3 and SWCNT/Pt:NH_3, NH_3 is strongly bound. In $SWCNT_{Vac}$/Pt:NH_3 and SWCNT/Pt:NH_3, ammonia is bound by 30.52 and 40.96 kcal/mol. The Pt–N distances are 2.29 and 2.14 Å, respectively. The strong binding of NH_3 to Pt via its nitrogen atom has a larger influence on the active region than the one caused by its

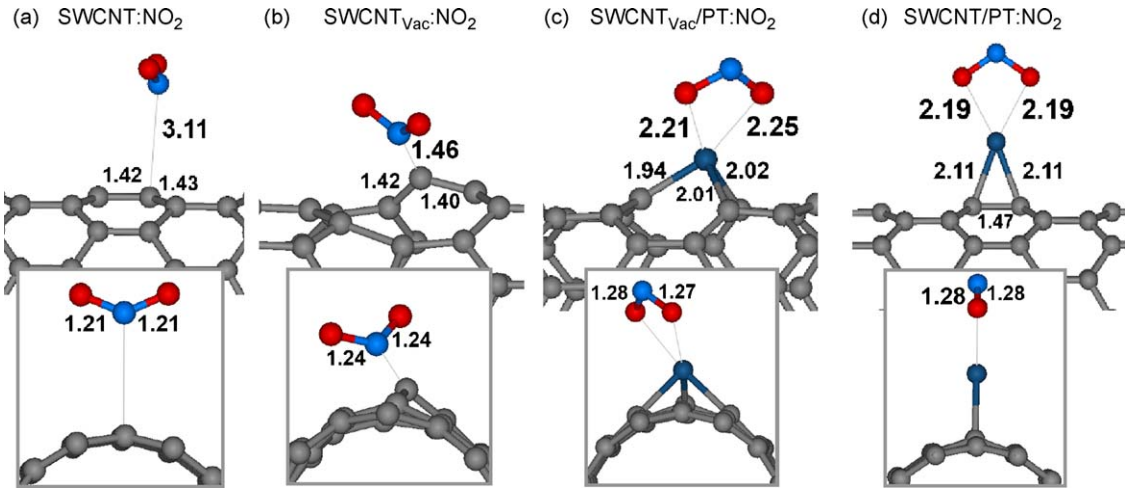

Fig. 2. Front and side views of the most favorable binding geometries of NO_2 on each support type, (a) pristine SWCNT, (b) vacancy SWCNT, (c) Pt-doped SWCNT and (d) Pt-deposited SWCNT, accompanied with their binding distances. Pt–C and some C–C distances (Å) are also given.

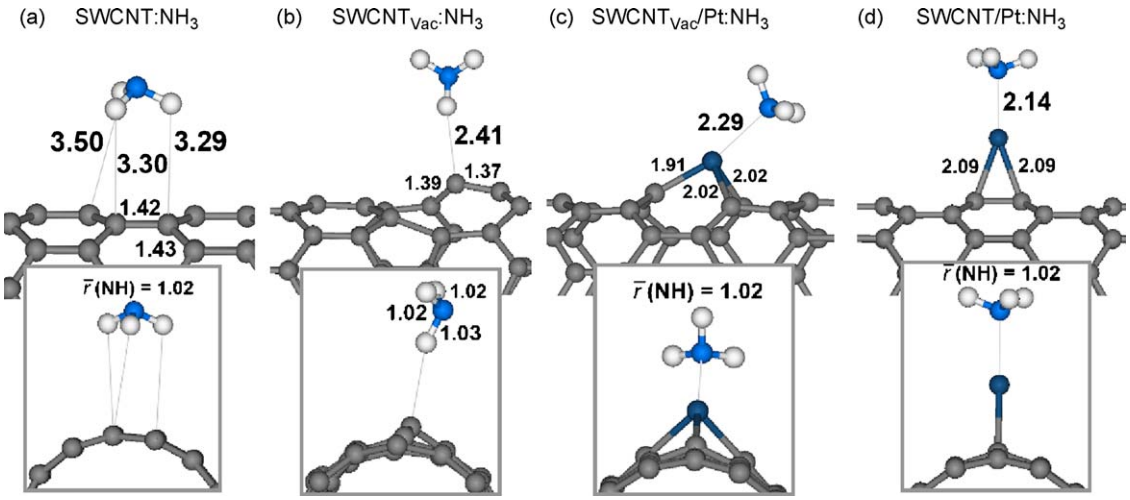

Fig. 3. Front and side views of the most favorable binding geometries of NH3 on each support type, (a) pristine SWCNT, (b) vacancy SWCNT, (c) Pt-doped SWCNT and (d) Pt-deposited SWCNT, accompanied with their binding distances. Pt–C and some C–C distances (Å) are also given..

weak H-bonded interaction with $SWCNT_{Vac}$, as can be seen from the redistribution of electron density (Fig. 4). As expected, the SWCNT–Pt distances increase somewhat from 2.05 Å to 2.09 Å after the NH_3 complexation. The N–H distances of all adsorbed NH_3 molecules are unaffected by the complexation and stay at 1.02 Å. The affinity of SWCNT/Pt to NH_3 approaches already the binding energy of the attached Pt to the SWCNT, which is a disadvantage since it might in practice lead to its destruction.

3.2. Electronic properties of the platform and sensitivity to NO_2 and NH_3

We investigated the effects of gas adsorption on the electronic properties of the SWCNTs by computing the charge transfers (q_{Gas}) between the gas molecule and support and the HOMO–LUMO energy gap modulations (ΔE_g). The results are summarized in Table 2. The quantities in this table are defined as:

$$\Delta E_g = E_g\,(\text{support : gas}) - E_g\,(\text{bare support})$$
$$\Delta q_{SWCNT} = q_{SWCNT}\,(\text{support : gas}) - q_{SWCNT}\,(\text{bare support})$$
$$\Delta q_{Pt} = q_{Pt}\,(\text{support : gas}) - q_{Pt}\,(\text{bare support})$$

In addition, electron densities difference maps HOMO and LUMO orbitals and electronic densities of states (DOSs) have been derived. They are depicted in Figs. 4–8.

3.2.1. NO_2

Since NO_2 is an electron-withdrawing molecule with an unusually large electron affinity between 2 eV and 3 eV [38], electrons are transferred from supports to it (Table 2). For $SWCNT_{Vac}$:NO_2, $SWCNT_{Vac}$/Pt:NO_2 and SWCNT/Pt:NO_2 these shifts amount to −0.27, −0.38 and −0.35*e*, respectively. The values for SWCNT/Pt:NO_2 and $SWCNT_{Vac}$/Pt:NO_2 are similar, but a more detailed analysis shows some differences. The positive value of Δq_{SWCNT} in $SWCNT_{Vac}$/Pt:NO_2 (0.32*e*) is larger than the one in SWCNT/Pt:NO_2 (0.22*e*). Three-dimensional plots of the differential electron density can give detailed information of the rearrangement of the complex formation. Fig. 4 shows isosurfaces of certain density changes. It can be seen that NO_2 adsorption (Fig. 4a–d) on $SWCNT_{Vac}$/Pt causes a depletion of electron density (Fig. 4c) throughout, which is expected to change the electric properties of the nanotube dramatically. In contrast, electron relocation in SWCNT/Pt:NO_2 occurs only locally at the Pt–NO_2 moiety. The change of the energy gap (ΔE_g) during the adsorption process is also related to the sensitivity of a sensor for a particular analyte. In Table 2, a negative sign of ΔE_g refers to a reduction of the energy gap in the complex compared to the bare support. We find that the energy gaps of all systems decrease after NO_2 adsorption by −0.32, −0.14, −0.25 and −0.41 eV for SWCNT:NO_2, $SWCNT_{Vac}$:NO_2, $SWCNT_{Vac}$/Pt:NO_2 and SWCNT/Pt:NO_2, respectively. This agrees

Table 2
Partial molecular and atomic charges $q(e)$ and values of the HOMO–LUMO gap E_g (eV) of all studied complexes. Partial charge transfers and energy gap changes are indicated by the prefix delta (Δ). Refer to text for the definitions of the quantities.

System	E_g	q_{SWCNT}	q_{Pt}
SWCNT	0.63	0.00	
$SWCNT_{Vac}$	0.26	0.00	
$SWCNT_{Vac}$/Pt	0.39	0.12	−0.12
SWCNT/Pt	0.58	0.05	−0.05

System	E_g	q_{SWCNT}	q_{Pt}	q_{Gas}	[a]ΔE_g	[b]Δq_{SWCNT}	[c]Δq_{Pt}
SWCNT:NO_2	0.31	0.05		−0.05	−0.32	0.05	
$SWCNT_{Vac}$:NO_2	0.12	0.27		−0.27	−0.14	0.27	
$SWCNT_{Vac}$/Pt:NO_2	0.14	0.44	−0.06	−0.38	−0.25	0.32	0.06
SWCNT/Pt:NO_2	0.17	0.27	0.08	−0.35	−0.41	0.22	0.13
SWCNT:NH_3	0.63	−0.01		0.01	0.00	−0.01	
$SWCNT_{Vac}$:NH_3	0.28	0.01		−0.01	0.02	0.01	
$SWCNT_{Vac}$/Pt:NH_3	0.29	−0.09	−0.18	0.27	−0.10	−0.21	−0.06
SWCNT/Pt:NH_3	0.62	−0.06	−0.22	0.28	0.04	−0.11	−0.17

[a] $\Delta E_g = E_g$ (support:gas) − E_g (bare support).
[b] $\Delta q_{SWCNT} = q_{SWCNT}$ (support:gas) − q_{SWCNT} (bare support).
[c] $\Delta q_{Pt} = q_{Pt}$ (support:gas) − q_{Pt} (bare support).

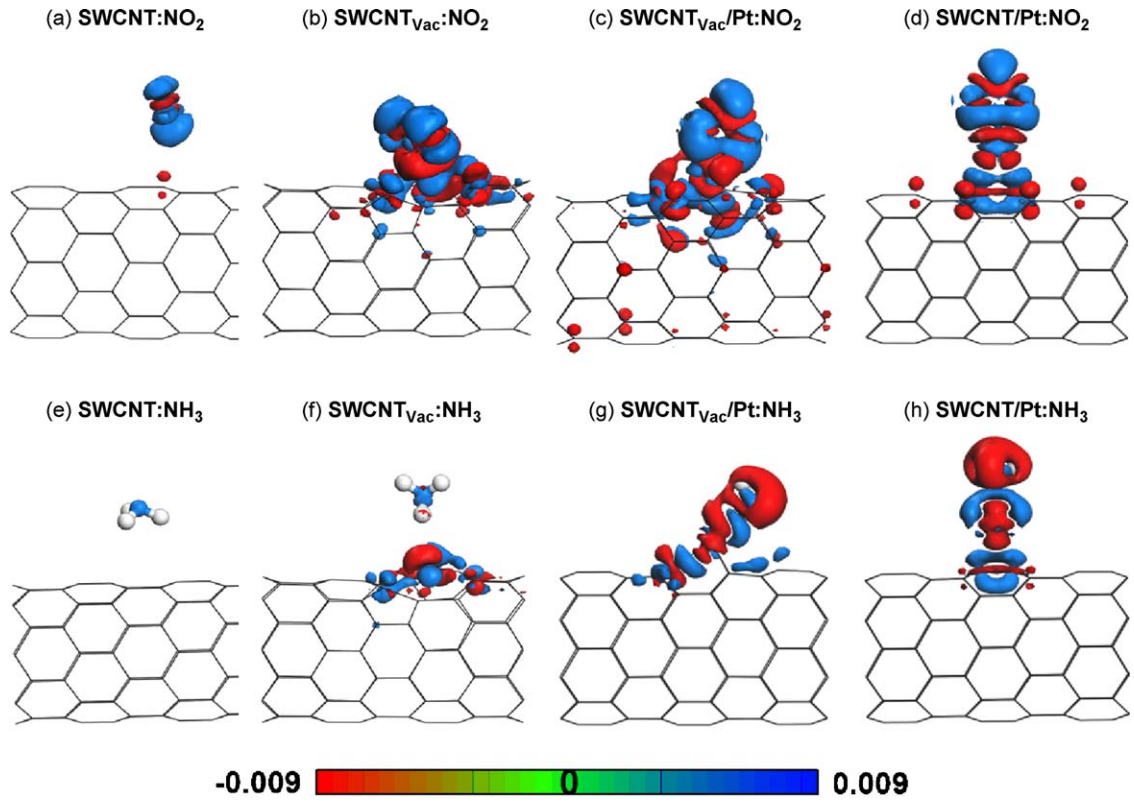

Fig. 4. Plots of the differential electron densities of all studied support-gas complexes, support-NO_2 complexes (a–d) and support-NH_3 complexes (e–h). The 3D-surfaces are plotted at isovalues of $\pm 0.009e/Å^3$. A red color denotes loss of density whereas blue denotes gain of electron density.

well with experimental reports that the conductivity of CNTs, defected-CNTs and Pt-doped–CNTs increase when exposed to NO_2 [1,4,14]. Electron density transfer to NO_2 generates holes in the support. The enhanced conductivities are directly related to the abundance of hole carriers, so these pristine and modified SWCNTs behave as p-type semiconductors as well and are also susceptible to become metallic after stimulated by NO_2, especially in the $SWCNT_{Vac}$:NO_2, $SWCNT_{Vac}$/Pt:NO_2 and SWCNT/Pt:NO_2 systems.

One can further see that the ΔE_g values are proportional to the amount of charge transfer, except for ΔE_g of SWCNT where NO_2 is very weakly bound. To clarify this further, we analyze the DOSs and PDOSs (Fig. 5). Comparing the DOS diagrams of SWCNT:NO_2 and SWCNT (Fig. 5e and a, respectively), one sees the appearance of an acceptor state in the middle of the HOMO–LUMO gap of the SWCNT, when NO_2 is bound [39]. When this state receives electrons from the valence band of the SWCNT the resistance of the system should decrease. Since this state is contributed from the NO_2 radical, as is indicated by the PDOSs and LUMO scheme of SWCNT:NO_2 (Figs. 5i and 6e, respectively), it is plausible that the measured energy gaps vary with the number of NO_2 molecules. SWCNT/Pt exhibits the highest change ΔE_g of its energy gap when NO_2 is bound to it (Table 2). However, that does not much affect the electronic structure of the SWCNT, as can be seen by the charge and electron density differences in Table 2 ($\Delta q_{SWCNT} = 0.22e$) and Fig. 4d, respectively. Moreover, the HOMO and LUMO orbitals (Fig. 6d and h, respectively), to which ΔE_g is related, have prominent contributions only in the area close to Pt and NO_2 and mostly involve the d-orbitals of Pt. Also the partial density of states distribution (Fig. 5n) shows the density near the Fermi level in SWCNT/Pt:NO_2 originating from these d-orbitals. The HOMO and LUMO of $SWCNT_{Vac}$/Pt:NO_2 (Fig. 6c and g, respectively) contain AO contributions from Pt and from the p-orbitals of the NO_2 oxygen atoms as well as from the nanotube mixed into the molecular orbitals of the whole system whereas in SWCN/Pt:NO_2, solely the first two and not the nanotube contribute to the frontier orbitals. Accordingly, despite the larger value of ΔE_g, in SWCNT/Pt:NO_2, its localized response to NO_2 binding makes it less suitable as a sensor.

3.2.2. NH_3

In this section we discuss the sensitivity of the three supports to NH_3 detecting. The lone pair electrons at the N atom of NH_3 can readily be donated to the molecule interacting with it. Consequently, the charge of adsorbed NH_3 is positive by 0.01, 0.27 and $0.28e$ in SWCNT:NH_3, $SWCNT_{Vac}$/Pt:NH_3 and SWCNT/Pt:NH_3, respectively, except for $SWCNT_{Vac}$:NH_3 ($-0.01e$) where C···H–N resembles a hydrogen bond and H–N behaves as the electron acceptor. The complexes with weak adsorption via the H atom, i.e. SWCNT:NH_3 and $SWCNT_{Vac}$:NH_3, also exhibit insignificant charge transfers of only 0.01 and $-0.01e$, respectively. Together with the unnoticeable electron density difference, the energy gap is also unchanged. This is associated with the bare SWCNT character of the PDOSs near the Fermi level (Fig. 7i and j) and is also visible in the HOMO–LUMO pictures of both complexes (Fig. 8a, b, e and f). This infers that SWCNT and $SWCNT_{Vac}$ have very low sensibility to NH_3 gas.

Extraordinary large charge transfers are found in $SWCNT_{Vac}$/Pt:NH_3 and SWCNT/Pt:NH_3 with values of 0.27 and $0.28e$, respectively. Amounts and directions of NH_3 charge transfer of both complexes are quite similar and also their electron density difference maps are similar as shown in Fig. 4g and h, respectively. The better efficiency is derived from the existence of the Pt active site and N-contacted mode which enhance the outflow of nitrogen lone pair electron density. Generally, giving up electrons from NH_3 to a p-type semiconductor support reduces the hole carrier density and thus decreases the conductivity of the system, correlated with the widening of its HOMO–LUMO gap [1]. Even though the flows of

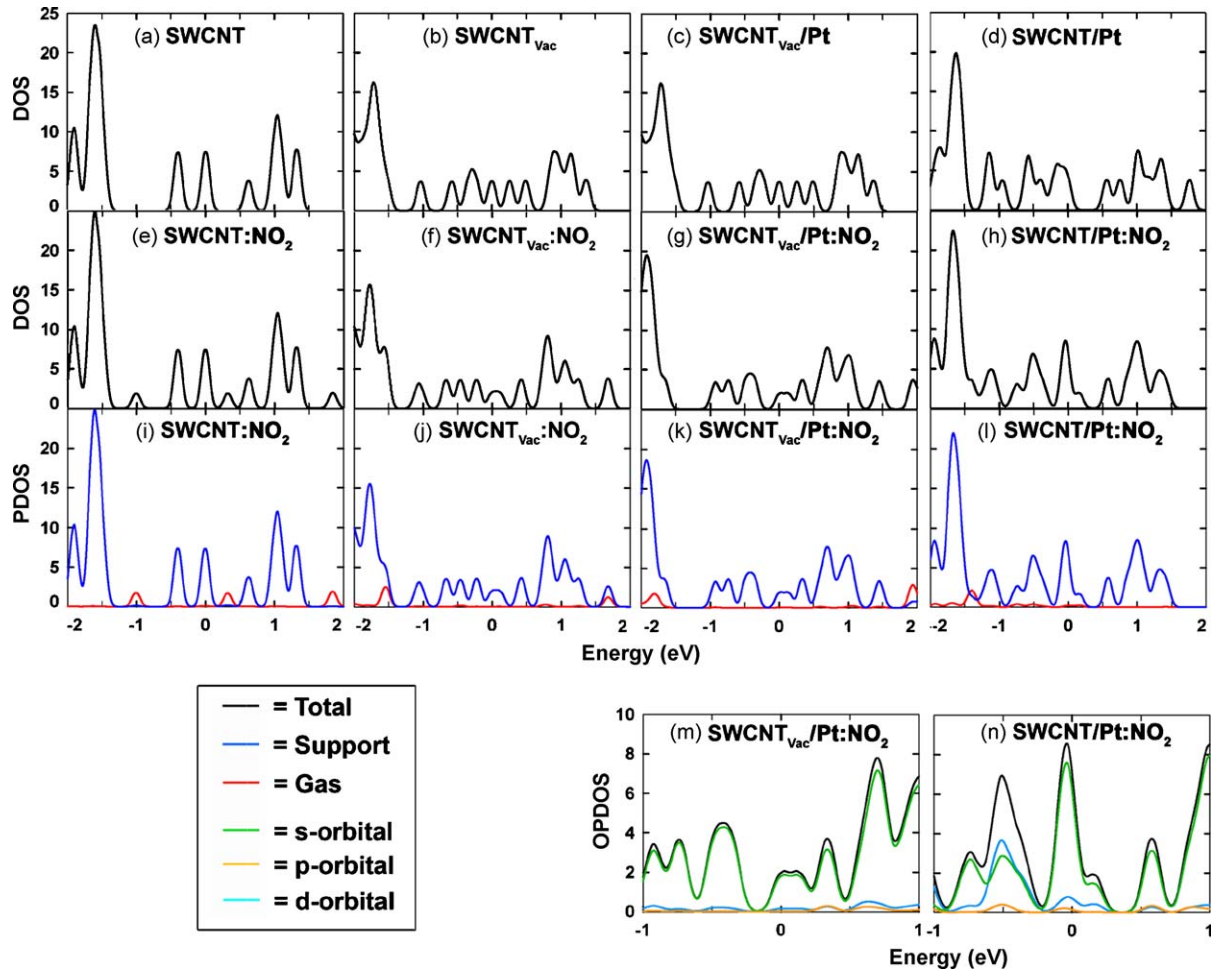

Fig. 5. Density of states (DOSs) for the studied supports (a–d) and their NO_2 complexes (e–h). Partial density of states (PDOSs) of all support-gas complexes (i–l) and orbital partial density of states (OPDOSs) of SWCNT$_{Vac}$/Pt:NO$_2$ and SWCNT/Pt:NO$_2$ (m and n) are also plotted for comparison. The Fermi levels (defined as the HOMO energies) are calibrated to locate at 0 eV.

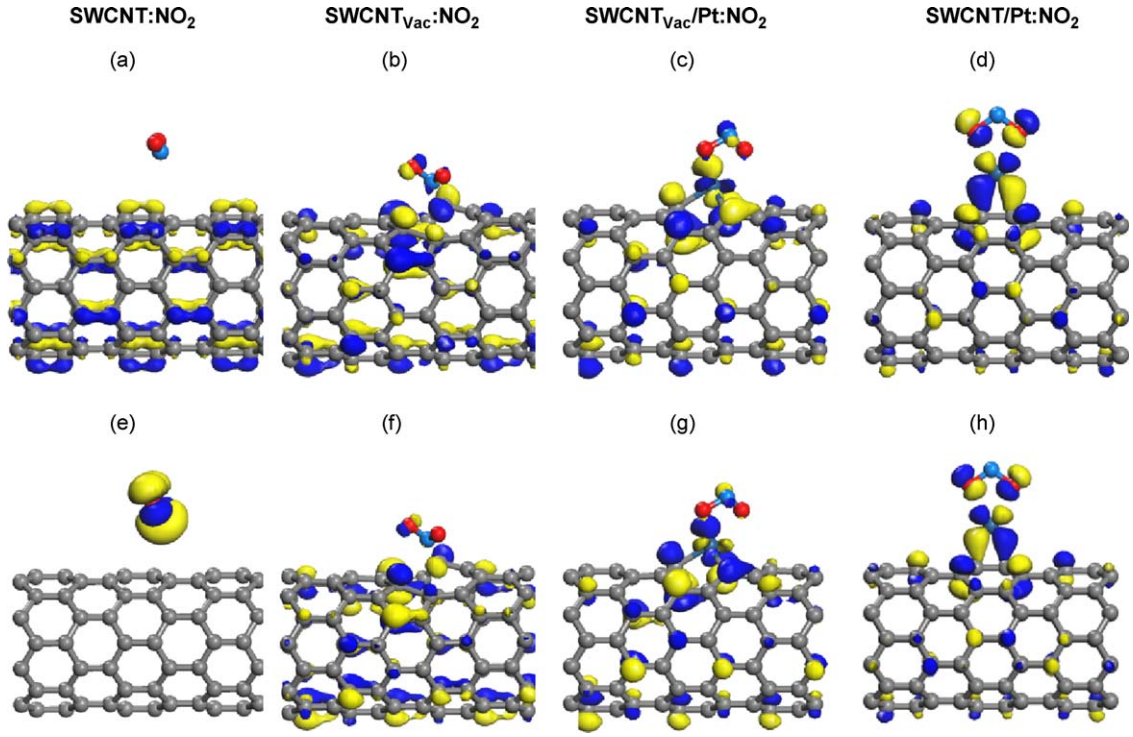

Fig. 6. Frontier molecular orbitals of the complexes with NO_2: HOMOs (a–d) and LUMOs (e–h).

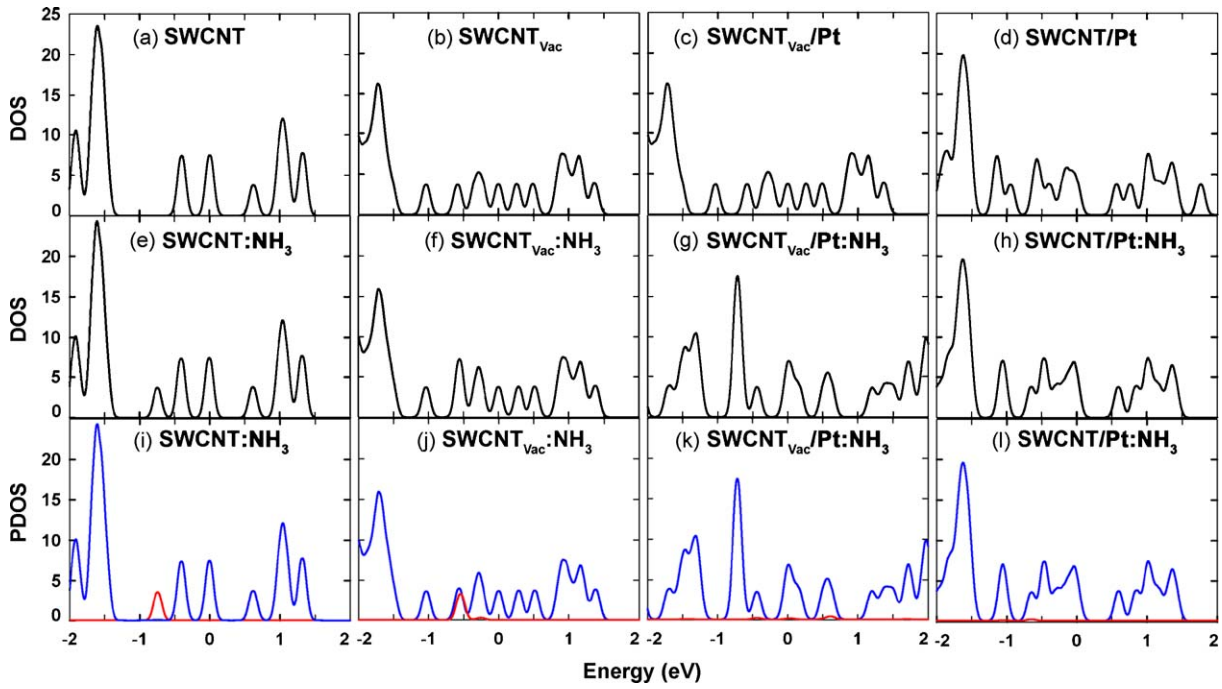

Fig. 7. Density of states (DOS) for all studied supports (a–d) and their NH_3 complexes (e–h). Partial density of states (PDOS) of all support-gas complexes (i–l) are also plotted for comparison (blue lines: support; red lines: contributions from NH_3). The Fermi levels (defined as HOMO energies) are calibrated to locate at 0 eV.

NH_3 electrons into $SWCNT_{Vac}/Pt:NH_3$ and $SWCNT/Pt:NH_3$ have the same direction, which indicates that they become less conductive, the signs of their ΔE_g values which represent how the conductivity changes are opposite. The energy gap of $SWCNT/Pt:NH_3$ is slightly widened (0.04 eV) whereas that of the $SWCNT_{Vac}/Pt:NH_3$ is significantly narrowed (−0.10 eV). These phenomena should principally interrelate to the electron redistribution in the support, especially of the SWCNT since the PDOSs near the Fermi level (Fig. 7k and l) and HOMO–LUMO features of both complexes (Fig. 8c, d, g and h) are merely contributed from it. Both Δq_{SWCNT} values of $SWCNT_{Vac}/Pt:NH_3$ and $SWCNT/Pt:NH_3$ are negative ($-0.21e$ and $-0.11e$, respectively) due to the accumulation of electrons in the SWCNTs. Remarkably, the $SWCNT_{Vac}/Pt:NH_3$ tube can receive twice the electron density than $SWCNT/Pt:NH_3$ does. This can change its electrical characteristic from p-type to n-type, which explains the observed increase in the conductivity after NH_3 adsorption. The reason for the poorer electron transfer to SWCNT in $SWCNT/Pt:NH_3$ is the weaker interaction between SWCNT and

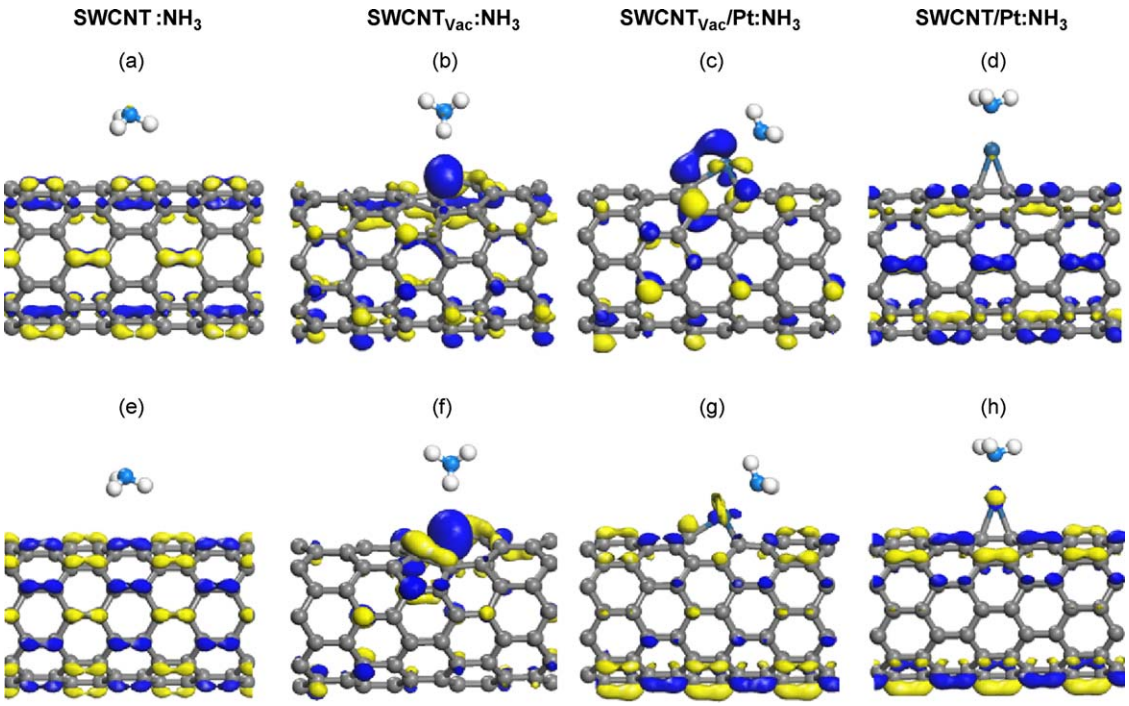

Fig. 8. Frontier molecular orbitals of all studied support-NH_3 complexes, HOMOs (a–d) and LUMOs (e–h).

Pt in the latter, which is further diminished by the adsorbed gas. The electron density acquired from NH_3 hardly moves to SWCNT as is shown by the accumulation of electron density on the Pt atom (Δq_{Pt}, $-0.17e$) after interacting with NH_3. Up until this point, $SWCNT_{Vac}$/Pt adequately satisfies the basic sensitivity requirements and induces more electronic change in terms of both the energy gap and partial charge transfer to the SWCNT than to the SWCNT/Pt.

4. Conclusion

We tried to study qualitatively the sensing performance of Pt–SWCNT with defective and pristine SWCNTs for NO_2 and NH_3 by means of first principle calculations. Overall, in both Pt-deposited and Pt-doped SWCNTs, platinum increases the charge transfer and other calculated properties. For the adsorption of NO_2, the Pt-doped SWCNT shows slightly smaller binding energies and gap changes than both the pristine SWCNT and the Pt-deposited SWCNT. Its electronic structure modulations are greater than that of the pristine SWCNT and its electron densities in the SWCNT unit are more disturbed than the ones of the Pt-deposited SWCNT. The binding of Pt to the SWCNT in the doped case is much stronger than if it is deposited on the surface. For NH_3 adsorption, the Pt-doped SWCNT shows the largest electron transfers to the SWCNT. We further compared the Pt-doped SWCNT with the well-known reactive defected SWCNT. Their abilities for capturing a NO_2 molecule are similar but for NH_3 the Pt-doped SWCNT is far better. The sensitivity of Pt-doped SWCNT is superior for both the detection of NO_2 and NH_3, because it exhibits larger energy gap changes and a larger charge transfer. These findings should be useful for the development of SWCNT-based nanosensor devices.

Acknowledgements

This research was supported by grants from the Thailand Research Fund to PP (Royal Golden Jubilee Ph.D. fellowship 3.C.KU/50/A.1) and to JL, the National Science and Technology Development Agency (NSTDA Chair Professor and NANOTEC Center of Excellence and CNC Consortium), the Kasetsart University Research and Development Institute (KURDI), and the Commission on Higher Education (Postgraduate Education and Research Programs in Petroleum, Petrochemicals and Advanced Materials). Support for CPU time on the Tera cluster of the Thai National Grid Center is also acknowledged.

Appendix A. Supplementary data

Supplementary data associated with this article can be found, in the online version, at doi:10.1016/j.jmgm.2009.04.005.

References

[1] J. Kong, N.R. Franklin, C. Zhou, M.G. Chapline, S. Peng, K. Cho, H. Dailt, Nanotube molecular wires as chemical sensors, Science 287 (5453) (2000) 622–625.
[2] H. Chang, J.D. Lee, S.M. Lee, Y.H. Lee, Adsorption of NH_3 and NO_2 molecules on carbon nanotubes, Appl. Phys. Lett. 79 (23) (2001) 3863–3865.
[3] S. Peng, K. Cho, P. Qi, H. Dai, Ab initio study of CNT NO_2 gas sensor, Chem. Phys. Lett. 387 (4–6) (2004) 271–276.
[4] S. Santucci, S. Picozzi, F. Di Gregorio, L. Lozzi, C. Cantalini, L. Valentini, J.M. Kenny, B. Delley, NO_2 and CO gas adsorption on carbon nanotubes: experiment and theory, J. Chem. Phys. 119 (20) (2003) 10904–10910.
[5] J. Lu, S. Nagase, Y. Maeda, T. Wakahara, T. Nakahodo, T. Akasaka, D. Yu, Z. Gao, R. Han, H. Ye, Adsorption configuration of NH_3 on single-wall carbon nanotubes, Chem. Phys. Lett. 405 (1–3) (2005) 90–92.
[6] L. Valentini, F. Mercuri, I. Armentano, C. Cantalini, S. Picozzi, L. Lozzi, S. Santucci, A. Sgamellotti, J.M. Kenny, Role of defects on the gas sensing properties of carbon nanotubes thin films: experiment and theory, Chem. Phys. Lett. 387 (4–6) (2004) 356–361.
[7] J. Andzelm, N. Govind, A. Maiti, Nanotube-based gas sensors—role of structural defects, Chem. Phys. Lett. 421 (1–3) (2006) 58–62.
[8] F. Mercuri, A. Sgamellotti, L. Valentini, I. Armentano, J.M. Kenny, Vacancy-induced chemisorption of NO_2 on carbon nanotubes. A combined theoretical and experimental study, J. Phys. Chem. B 109 (27) (2005) 13175–13179.
[9] L. Bai, Z. Zhou, Computational study of B- or N-doped single-walled carbon nanotubes as NH_3 and NO_2 sensors, Carbon 45 (10) (2007) 2105–2110.
[10] S. Peng, K. Cho, Ab initio study of doped carbon nanotube sensors, Nano Lett. 3 (4) (2003) 513–517.
[11] R. Wang, D. Zhang, W. Sun, Z. Han, C. Liu, A novel aluminum-doped carbon nanotubes sensor for carbon monoxide, Theochem 806 (1–3) (2007) 93–97.
[12] R. Wang, D. Zhang, Y. Zhang, C. Liu, Boron-doped carbon nanotubes serving as a novel chemical sensor for formaldehyde, J. Phys. Chem. B 110 (37) (2006) 18267–18271.
[13] A. Star, V. Joshi, S. Skarupo, D. Thomas, J.-C.P. Gabriel, Gas sensor array based on metal-decorated carbon nanotubes, J. Phys. Chem. B 110 (42) (2006) 21014–21020.
[14] M. Penza, G. Cassano, R. Rossi, M. Alvisi, A. Rizzo, M.A. Signore, T. Dikonimos, E. Serra, R. Giorgi, Enhancement of sensitivity in gas chemiresistors based on carbon nanotube surface functionalized with noble metal (Au, Pt) nanoclusters, App. Phys. Lett. 90 (17) (2007) 173123/1–173123/3.
[15] S. Mubeen, T. Zhang, B. Yoo, M.A. Deshusses, N.V. Myung, Palladium nanoparticles decorated single-walled carbon nanotube hydrogen sensor, J. Phys. Chem. C 111 (17) (2007) 6321–6327.
[16] M.K. Kumar, S. Ramaprabhu, Nanostructured Pt functionlized multiwalled carbon nanotube based hydrogen sensor, J. Phys. Chem. B 110 (23) (2006) 11291–11298.
[17] S.J. Kim, Y.J. Park, E.J. Ra, K.K. Kim, K.H. An, Y.H. Lee, J.Y. Choi, C.H. Park, S.K. Doo, M.H. Park, C.W. Yang, Defect-induced loading of Pt nanoparticles on carbon nanotubes, App. Phys. Lett. 90 (2) (2007) 023114/1–023114/3.
[18] C. Zhou, J. Wu, A. Nie, R.C. Forrey, A. Tachibana, H. Cheng, On the sequential hydrogen dissociative chemisorption on small platinum clusters: a density functional theory study, J. Phys. Chem. C 111 (34) (2007) 12773–12778.
[19] L.C. Grabow, A.A. Gokhale, S.T. Evans, J.A. Dumesic, M. Mavrikakis, Mechanism of the water gas shift reaction on Pt: first principles, experiments, and microkinetic modeling, J. Phys. Chem. C 112 (12) (2008) 4608–4617.
[20] Y. Wang, P.B. Balbuena, Roles of proton and electric field in the electroreduction of O_2 on Pt(1 1 1) surfaces: results of an ab-initio molecular dynamics study, J. Phys. Chem. B 108 (14) (2004) 4376–4384.
[21] H. Orita, Y. Inada, DFT investigation of CO adsorption on Pt(2 1 1) and Pt(3 1 1) surfaces from low to high coverage, J. Phys. Chem. B 109 (47) (2005) 22469–22475.
[22] B. Delley, An all-electron numerical method for solving the local density functional for polyatomic molecules, J. Chem. Phys. 92 (1) (1990) 508–517.
[23] B. Delley, From molecules to solids with the $DMol^3$ approach, J. Chem. Phys. 113 (18) (2000) 7756–7764.
[24] T. Strassner, M.A. Taige, Evaluation of functionals O3LYP, KMLYP, and MPW1K in comparison to B3LYP for selected transition-metal compounds, J. Chem. Theory Comput. 1 (5) (2005) 848–855.
[25] Z. Slanina, P. Pulay, S. Nagase, H_2, Ne, and N_2 energies of encapsulation into C60 evaluated with the MPWB1K functional, J. Chem. Theory Comput. 2 (2006) 782–785.
[26] S.G. Stepanian, M.V. Karachevtsev, A.Yu. Glamazda, V.A. Karachevtsev, L. Adamowicz, Stacking interaction of cytosine with carbon nanotubes: MP2, DFT and Raman spectroscopy study, Chem. Phys. Lett. 459 (2008) 153–158.
[27] J.P. Perdew, Y. Wang, Accurate and simple analytic representation of the electron-gas correlation energy, Phys. Rev. B 45 (23) (1992) 13244–13249.
[28] B. Delley, Hardness conserving semilocal pseudopotentials, Phys. Rev. B: Condens. Matter Mater. Phys. 66 (15) (2002) 155125/1–155125/9.
[29] H.J. Monkhorst, J.D. Pack, Special points for Brillouin-zone integrations, Phys. Rev. B 13 (12) (1976) 5188–5192.
[30] O. Gulseren, T. Yildirim, S. Ciraci, Systematic ab initio study of curvature effects in carbon nanotubes, Phys. Rev. B: Condens. Matter Mater. Phys. 65 (15) (2002) 153405/1–153405/4.
[31] X. Blase, L.X. Benedict, E.L. Shirley, S.G. Louie, Hybridization effects and metallicity in small radius carbon nanotubes, Phys. Rev. Lett. 72 (12) (1994) 1878–1881.
[32] D. Vanderbilt, Soft self-consistent pseudopotentials in a generalized eigenvalue formalism, Phys. Rev. B 41 (11) (1990) 7892–8795.
[33] V. Milman, B. Winkler, J.A. White, C.J. Pickard, M.C. Payne, E.V. Akhmatskaya, R.H. Nobes, Electronic structure, properties, and phase stability of inorganic crystals: a pseudopotential plane-wave study, Int. J. Quantum Chem. 77 (5) (2000) 895–910.
[34] E. Durgun, S. Dag, V.M.K. Bagci, O. Gulseren, T. Yildirim, S. Ciraci, Systematic study of adsorption of single atoms on a carbon nanotube, Phys. Rev. B: Condens. Matter Mater. Phys. 67 (20) (2003) 201401/1–201401/4.
[35] G. Chen, Y. Kawazoe, Interaction between a single Pt atom and a carbon nanotube studied by density functional theory, Phys. Rev. B: Condens. Matter Mater. Phys. 73 (12) (2006) 125410/1–125410/6.
[36] L.Y. Chiang, J.B. Bhonsle, L. Wang, S.F. Shu, T.M. Chang, J.R. Hwu, Efficient one-flask synthesis of water-soluble [60]fullerenols, Tetrahedron 52 (14) (1996) 4963–4972.
[37] Z. Slanina, X. Zhao, L.Y. Chiang, E. Osawa, Biologically active fullerene derivatives: computations of structures, energetics, and vibrations of C60(OH)X and C60(NO_2)Y, Int. J. Quantum Chem. 74 (3) (1999) 343–349.
[38] The National Institute of Standards and Technology (NIST): Standard Reference Data Program (Chemistry WebBook, http://webbook.nist.gov).
[39] Y. Zhang, C. Suc, Z. Liu, J. Li, Carbon nanotubes functionalized by NO_2: coexistence of charge transfer and radical transfer, J. Phys. Chem. B 110 (45) (2006) 22462–22470.